Check for updates

ADVANCED MATERIALS
www.advmat.de

A Fiber Sensor for Long-Term Monitoring of Extracellular Potassium Ion Fluctuations in Chronic Neuropsychiatric Diseases

Jiajia Wang, Liyuan Wang, Yiqing Yang, HongJian Li, Xinlin Huang, Ziwei Liu, Sihui Yu, Chengqiang Tang, Jiawei Chen, Xiang Shi, Wenjun Li, Peining Chen, Qi Tong, Hongbo Yu, Xuemei Sun, and Huisheng Peng**

The extracellular potassium ion concentration in the brain exerts a significant influence on cellular excitability and intercellular communication. Perturbations in the extracellular potassium ion level are closely correlated with various chronic neuropsychiatric disorders including depression. However, a critical gap persists in performing real-time and long-term monitoring of extracellular potassium ions, which is necessary for comprehensive profiling of chronic neuropsychiatric diseases. Here, a fiber potassium ion sensor (FKS) that consists of a soft conductive fiber with a rough surface and a hydrophobic-treated transduction layer interfaced with a potassium ion-selective membrane is found to solve this problem. The FKS demonstrates stable interfaces between its distinct functional layers in an aqueous environment, conferring an exceptional stability of 6 months in vivo, in stark contrast to previous reports with working durations from hours to days. Upon implantation into the mouse brain, the FKS enables effective monitoring of extracellular potassium ion dynamics under diverse physiological states including anesthesia, forced swimming, and tail suspension. Using this FKS, tracking of extracellular potassium ion fluctuations that align with behaviors associated with the progression of depression over months is achieved, demonstrating its usability in studying chronic neuropsychiatric disorders from a new biochemical perspective.

1. Introduction

The potassium ion (K^+), as an important vehicle for transmembrane transport, constitutes the cornerstone of cellular vitality and operations throughout the entirety of an organism.[1] In the active milieu of the brain, K^+ plays an irreplaceable role in mediating neural activities and facilitating brain functionalities.[2] However, dysfunction of K^+ channels across cellular membranes can disrupt the transport of K^+, resulting in abnormal extracellular K^+ levels ($[K^+]_e$). These abnormalities have been intimately correlated with an array of neuropsychiatric diseases such as Huntington's disease, Parkinson's disease, Alzheimer's disease, and depression[3] (**Figure 1a**). Therefore, monitoring $[K^+]_e$ and its fluctuations in the brain represent an efficient strategy to provide new insights into the etiology and therapeutic avenues of neuropsychiatric diseases.

Methods exist for real-time monitoring of $[K^+]_e$ in the brains of animals. Conventional microdialysis provides exquisite resolution for $[K^+]_e$ monitoring with a working time over days in vivo.[4] Optical devices by combining optical fiber with fluorescent/near-infrared K^+ nanosensors enable the monitoring of the changes in $[K^+]_e$ within a few hours.[5] Glassy liquid and solid contact electrochemical K^+ sensors have been miniaturized to allow implantation and $[K^+]_e$ monitoring for periods of hours to days.[2a,3c,6] However, animal models designed to replicate and decipher chronic neuropsychiatric diseases are always sustained for months.[7] Regrettably, these available methods are far from the requirements for long-term monitoring of the level of or fluctuation in $[K^+]_e$ in the brain during chronic neuropsychiatric diseases (Figure 1b and Tables S1 and S2, Supporting Information).

Here, we report a fiber electrochemical K^+ sensor (FKS) with stability up to 6 months in the brain, matching the durations of chronic neuropsychiatric diseases. The FKS was constructed by leveraging a carbon nanotube fiber (CNTF) with a rough surface and hydrophobic-treated poly(3,4-ethylenedioxythiophene):poly(styrenesulfonate) (PEDOT:PSS) (HT-PP) to stably interface with a K^+-selective membrane

J. Wang, L. Wang, Y. Yang, X. Huang, Z. Liu, S. Yu, C. Tang, J. Chen, X. Shi, W. Li, P. Chen, X. Sun, H. Peng
State Key Laboratory of Molecular Engineering of Polymers
Department of Macromolecular Science
Institute of Fiber Materials and Devices
and Laboratory of Advanced Materials
Fudan University
Shanghai 200438, China
E-mail: sunxm@fudan.edu.cn; penghs@fudan.edu.cn

H. Li, H. Yu
Vision Research Laboratory
School of Life Sciences
State Key Laboratory of Medical Neurobiology
Collaborative Innovation Center for Brain Science
Fudan University
Shanghai 200438, China

Q. Tong
Department of Aeronautics and Astronautics
Fudan University
Shanghai 200433, China

The ORCID identification number(s) for the author(s) of this article can be found under https://doi.org/10.1002/adma.202309862

DOI: 10.1002/adma.202309862

 © 2023 Wiley-VCH GmbH

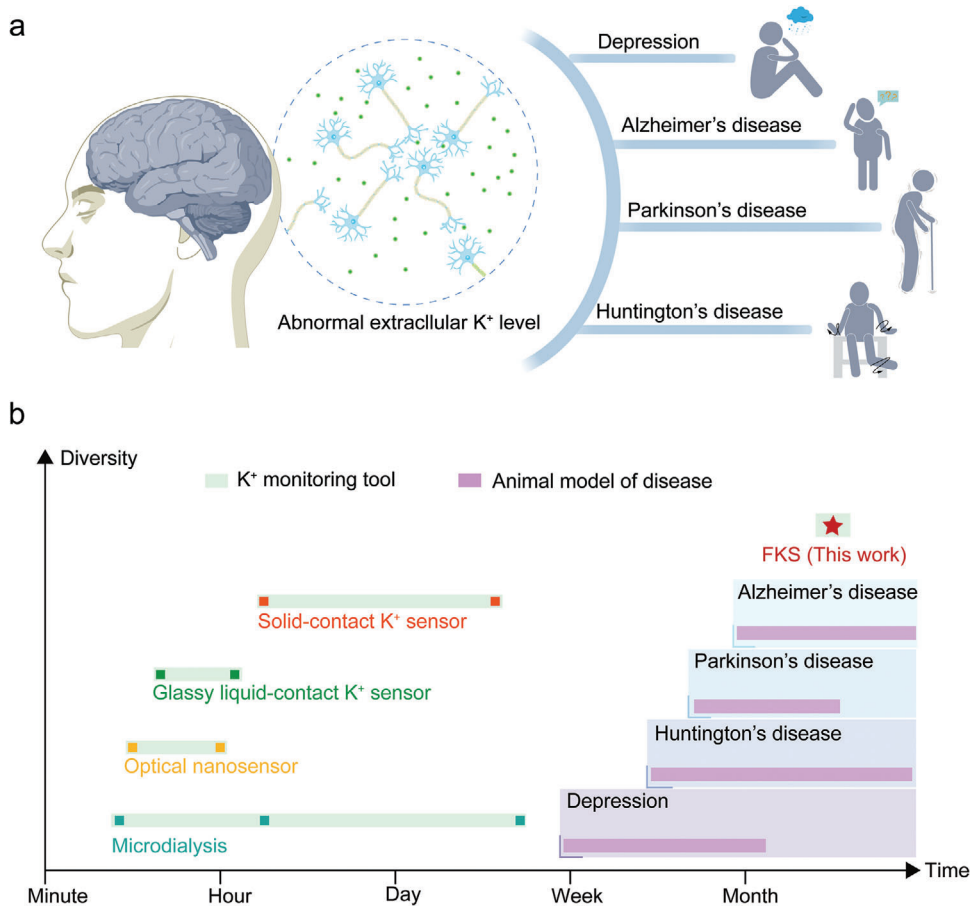

Figure 1. Comparison of the timescales of K^+ monitoring tools and neuropsychiatric diseases. a) Conceptual illustration of abnormal extracellular K^+ levels in the brain and the related chronic neuropsychiatric diseases to demonstrate the requirement of long-term monitoring of K^+ levels in time. b) Typical timescales of both the lifetime of real-time K^+ monitoring tools in the brain and durations of animal models of neuropsychiatric diseases. The lifetime of the FKS is superior to that in previous reports and matches the durations of the animal models of neuropsychiatric diseases.

(Figure S1a,b, Supporting Information). The fabricated FKS with a diameter of ≈60 μm minimized invasiveness during implantation (Figure S1c,d, Supporting Information). After implantation in the mouse brain, the FKS recorded the changes in $[K^+]_e$ during neuronal excitation and inhibition. Furthermore, the FKS showed dynamic changes in $[K^+]_e$ consistent with the behavioral manifestation over the onset period of depression, exhibiting its ability to serve as a powerful biochemical tool to understand neuropsychiatric diseases.

2. Results and Discussion

An electrochemical K^+ sensor typically consists of three layers, that is, a conductive substrate, a transduction layer, and a K^+-selective membrane. A stable interface between the transduction layer and the K^+-selective membrane is one of the key determinants of long-term stability. Specifically, based on the phase-boundary detection mechanism,[8] when K^+ is recognized by the K^+-selective membrane, ion exchangers within the membrane will cross the interface between the K^+-selective membrane and the transduction layer, driving the redox reaction of the transduction layer and the subsequent potential change of the electrode. With prolonged time in an aqueous environment, water tends to accumulate and forms a water layer at the interface between the K^+-selective membrane and the transduction layer, which will disturb ion migration, thereby causing potential drift and deteriorating the performance of the K^+ sensor. Therefore, we aimed to construct a stable interface between the transduction layer and the K^+-selective membrane to prevent the formation of a water layer and ensure effective ion migration throughout prolonged usage.

The hydrophobic features of both the transduction layer and the K^+-selective membrane play a pivotal role in constructing a stable interface. Typically, the K^+-selective membrane based on a poly(vinyl chloride) matrix exhibits a nearly hydrophobic nature, while the widely used transduction layer PEDOT:PSS lacks hydrophobicity due to the abundant presence of PSS. Hence, enhancing the hydrophobicity of the transduction layer becomes a crucial consideration. To address this, we adopted a dual-pronged strategy that involved both the design of a rough surface and the reduction of hydrophilic components (**Figure 2a**), considering that the morphology and intrinsic components are the two decisive factors influencing hydrophobicity.[9]

© 2023 Wiley-VCH GmbH

15214095, 2024, 13, Downloaded from https://onlinelibrary.wiley.com/doi/10.1002/adma.202309862 by Fudan University, Wiley Online Library on [06/12/2024]. See the Terms and Conditions (https://onlinelibrary.wiley.com/terms-and-conditions) on Wiley Online Library for rules of use; OA articles are governed by the applicable Creative Commons License

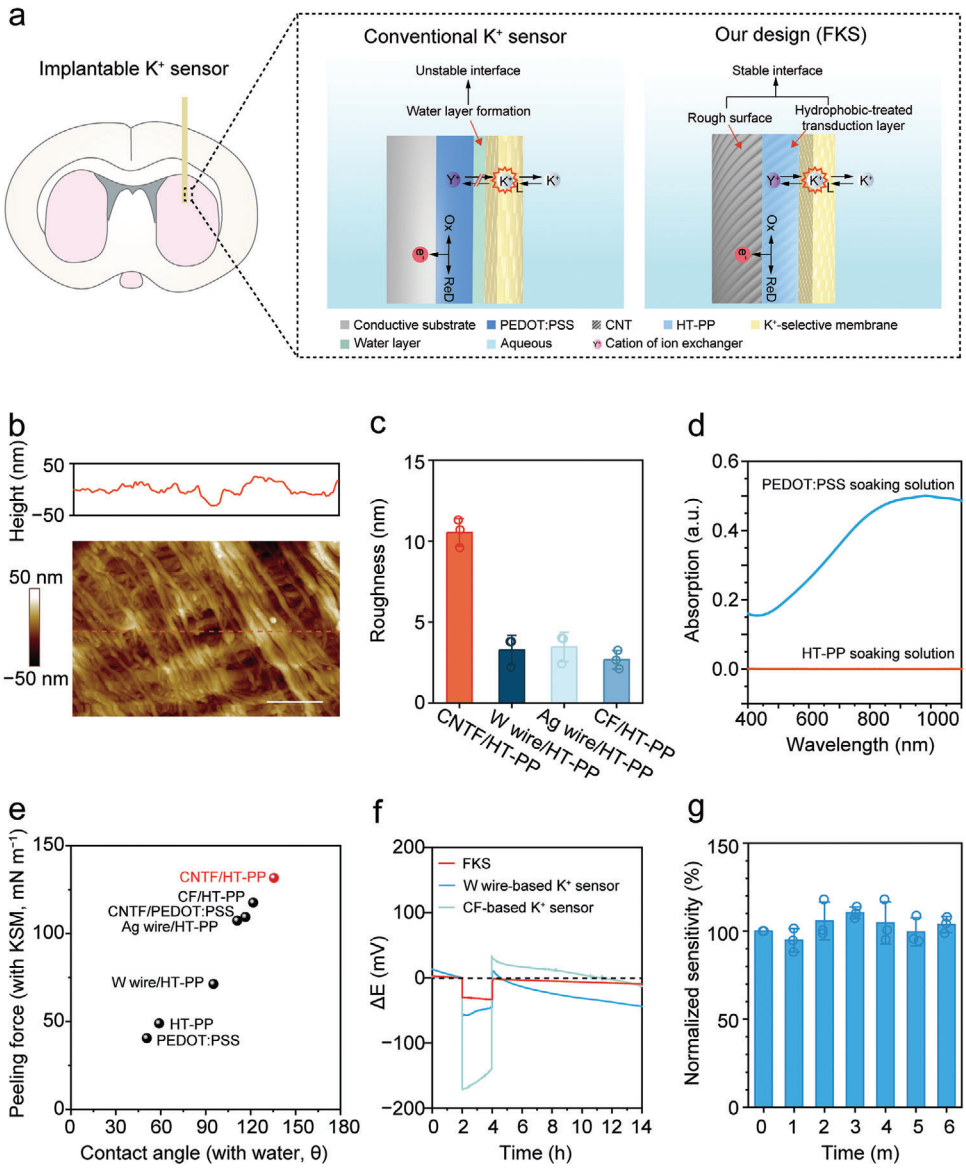

Figure 2. Interface design and performance of the FKS. a) Interface design of the conventional K^+ sensor (left) and our FKS (right). For implantable K^+ sensors, the degradation of conventional K^+ sensors is mainly attributed to water layer formation between the transduction layer and the selective membrane. Our design enables a stable interface inside the FKS by creating a rough surface and a hydrophobic-treating transduction layer to impede water accumulation. L represents an ionophore. b) Atomic force microscopy image of CNTF/HT-PP (bottom) and corresponding height along the orange dashed line (top). The results show that the twisted fiber structure brought a rough surface. Scale bar, 600 nm. c) Roughness of CNTF/HT-PP, tungsten (W) wire/HT-PP, silver (Ag) wire/HT-PP, and carbon fiber (CF)/HT-PP ($n = 3$, mean ± s.d.). The surface of CNTF/HT-PP is much rougher than that of the others. d) UV–vis absorption spectra of the solutions after PEDOT:PSS and HT-PP soaking for 24 h showing the water stability of HT-PP. The UV–vis absorption corresponding to the π–π transition in PEDOT occurs over a broad range and peaks at ≈800 nm. e) Peeling forces for separating the K^+-selective membrane (KSM) from transduction layers with different water contact angles. CNTF/HT-PP shows the highest hydrophobicity and peeling force. f) Water layer test for the FKS and W wire/HT-PP-based and CF/HT-PP-based K^+ sensors. The FKS exhibits the least potential drift. The tests were implemented in KCl for 2 h, NaCl for 2 h, and back to KCl for 10 h, and all solutions had a concentration of 0.1 M. g) Sensitivities of the FKS kept in artificial cerebrospinal fluid for 6 months, exhibiting long-term stability ($n = 3$, mean ± s.d.).

Here, the FKS utilized a CNTF with a rough surface as the conductive substrate and HT-PP as the transduction layer to contact the K^+-selective membrane. The CNTF electrode twisted from carbon nanotubes showed a notable roughness of ≈10.6 nm, much higher than those of planar substrates, traditional metal wire, and carbon fiber electrodes that are commonly used in implantable ion sensors, and the roughness was retained after being modified with the transduction layer (Figure 2b,c and Figures S2 and S3 and Table S3, Supporting Information). Meanwhile, the PEDOT:PSS layer was treated with an ionic liquid and dimethylsulfoxide, resulting in a reduction of the PSS/PEDOT ratio from 2.44 to 1.37 in HT-PP (Figure S4a, Supporting Information). Both the PEDOT:PSS and HT-PP layers were soaked in water for 24 h to examine their stability. The solution after

© 2023 Wiley-VCH GmbH

15214095, 2024, 13, Downloaded from https://onlinelibrary.wiley.com/doi/10.1002/adma.202309862 by Fudan University, Wiley Online Library on [06/12/2024]. See the Terms and Conditions (https://onlinelibrary.wiley.com/terms-and-conditions) on Wiley Online Library for rules of use; OA articles are governed by the applicable Creative Commons License

PEDOT:PSS soaking showed obvious UV–vis absorption corresponding to PEDOT at ≈800 nm, while that after HT-PP soaking showed almost no absorption, indicating greatly improved aqueous stability (Figure 2d and Figure S4b, Supporting Information). Furthermore, Raman spectra showed strong interactions between the CNTF and the HT-PP layer (Figure S4c, Supporting Information). Even after thousands of cyclic voltammetry cycles in phosphate-buffered saline, the HT-PP layer on the CNTF (CNTF/HT-PP) remained stable (Figure S4d, Supporting Information). Finally, with the combination of a rough surface and hydrophobic treatment, CNTF/HT-PP showed enhanced hydrophobicity, with an increase in the water contact angle from 50° (PEDOT:PSS) to 135°, while the HT-PP layer on metal wire and carbon fiber with smoother surfaces and CNTF/PEDOT:PSS without hydrophobic treatment demonstrated water contact angles of 95°–121° and 116°, respectively (Table S4, Supporting Information). Besides, other widely used transduction layers modified on the surface of CNTF showed water contact angles of 69°–128° (Table S5, Supporting Information).

We further evaluated the contribution of the hydrophobicity to the interfacial stability. The peeling force to separate the transduction layer and the K^+-selective membrane in an aqueous environment was determined from the measured contact angles. Remarkably, the CNTF/HT-PP exhibited the largest peeling force (131.58 mJ m^{-2}) with the K^+-selective membrane compared with the other transduction layers (Figure 2e). The increased hydrophobicity was indeed conducive to a larger peeling force. Importantly, the resulting FKS demonstrated negligible potential drift when it was switched from K^+ to Na^+ solutions and back to K^+ solution, while much larger potential drifts were found in the sensors based on metal wire and carbon fiber (Figure 2f). Upon changing the solution, the transport of relevant ions across the membrane into the water layer or the reverse process would change the ionic composition in the water layer, driving to establish a new equilibrium and leading to the potential drift.[8a,10] Therefore, the potential drift results suggested that a minimal water layer formed at the interface inside the FKS. Taken together, we successfully constructed a stable interface between the transduction layer and the K^+-selective membrane, which laid a robust foundation for the long-term stability of the FKS.

We then examined the sensing properties of the FKS to evaluate its capability for long-term monitoring of K^+ fluctuations. Basically, the FKS showed a sensitivity of 52.8 mV lg^{-1} [K^+] near the ideal Nernstian response, a low detection limit of 3.5 μM, and good reversibility of the potential response to varying K^+ concentration (Figure S5a–c, Supporting Information). The FKS also exhibited an excellent temporal resolution of 0.3 s (Figure S5d, Supporting Information). The potential response of the FKS to K^+ was much higher than that to other interfering ions (Na^+, Ca^{2+}, and Mg^{2+}) (Figure S5e, Supporting Information), revealing its high selectivity to ensure detection accuracy. Such favorable performance enabled the FKS to effectively monitor reversible changes in $[K^+]_e$ related to rapid neural activities at the micromolar level.[1,11] The FKS also illustrated an anti-biofouling ability, as the sensitivity remained stable after soaking in 10 mg mL^{-1} bovine serum albumin for 12 h (Figure S5f, Supporting Information). Most importantly, due to the design of a stable interface, the sensitivity of the FKS was maintained at 93% after 6 months in the simulated brain environment, while the other sensors based on metal wire and carbon fiber dramatically declined in sensitivity within the first month (Figure 2g and Figure S5g,h, Supporting Information).

For implantable sensors, mechanical matching between the sensor and the surrounding tissue is beneficial to avoid their relative displacement and then form a stable and biocompatible interface.[12] For the K^+ sensor, Young's modulus of the CNTF used in the FKS was ≈65 MPa, much lower than that of the other substrates, such as tungsten wire and carbon fiber, while closer to the brain (Figure S6a, Supporting Information). Moreover, employing finite element analysis, the CNTF demonstrated a more modest and uniformly distributed internal stress profile during deformation compared with the other types of fiber electrodes (Figure S6b, Supporting Information). Furthermore, from the 3D finite element analysis model for implanting fibers in brain tissue, minimal stress appeared at the interface between the CNTF and the brain, and the displacement of the CNTF was consistent with that of brain tissue during micromotion (Figure S6c–g, Supporting Information). Hence, a mechanically matched stable interface could be established between the FKS and the brain tissue to reduce tissue damage and foster long-term stability.

The biocompatibility of the FKS was further evaluated by characterizing the distribution of cells, especially immune cells, surrounding the implantation site. Fluorescence images and measured fluorescence intensities indicated minimal encapsulation by immune cells and negligible neuron loss around the implantation site for 1 month after implantation of the FKS, similar to the control group without FKS implantation (Figure S7a–h, Supporting Information). These results demonstrated a favorable biocompatibility of the FKS.

The FKS was implanted into the hippocampus of a mouse brain to monitor the fluctuations in $[K^+]_e$ (**Figure 3a**). Concurrently, a neural probe constructed from the CNTF was also implanted to record electrophysiological signals to assess the excitability of cells. To regulate the cellular excitability and induce $[K^+]_e$ fluctuations, we applied various concentrations of anesthetic (isoflurane). As the anesthetic concentration shifted from 2% ($V_{isoflurane}$: V_{air}) to 0.5%, the rising potential of the FKS revealed a trend of increasing $[K^+]_e$, accompanied by enhanced amplitudes and power densities of electrophysiological signals, exhibiting more active cellular activities. Adjusting the anesthetic concentration back to 2% led to a decrease in both $[K^+]_e$ and the excitability of cells (Figure 3b). The changes in $[K^+]_e$ detected by the FKS conformed to the influx/outflux dynamics of K^+ in the brain.

The temporal relationship between $[K^+]_e$ fluctuations and transitions in cellular excitability was further investigated. We collected dozens of FKS potential changes ($\Delta E_{[K^+]_e}$) in response to $[K^+]_e$ fluctuations and $\Delta E_{[K^+]_e}$ showed the same tendency under the regulation of the anesthetic (Figure 3c). The alteration times of $[K^+]_e$ and the cellular excitability were obtained from the slope of $\Delta E_{[K^+]_e}$ and the firing rate of electrophysiological signals, respectively. In an experimental case where the anesthetic concentration was changed at 0 and 600 s, we observed a significant increase in $[K^+]_e$ at ≈40 s and a decrease at ≈630 s (Figure 3di). Correspondingly, the cells displayed a gradual excitation at ≈50 s and subsequent inhibition at ≈620 s (Figure 3dii). With the same calculation method, we systematically analyzed all recordings from both the FKS and neural probes to establish the temporal

© 2023 Wiley-VCH GmbH

15214095, 2024, 13, Downloaded from https://onlinelibrary.wiley.com/doi/10.1002/adma.202309862 by Fudan University, Wiley Online Library on [06/12/2024]. See the Terms and Conditions (https://onlinelibrary.wiley.com/terms-and-conditions) on Wiley Online Library for rules of use; OA articles are governed by the applicable Creative Commons License

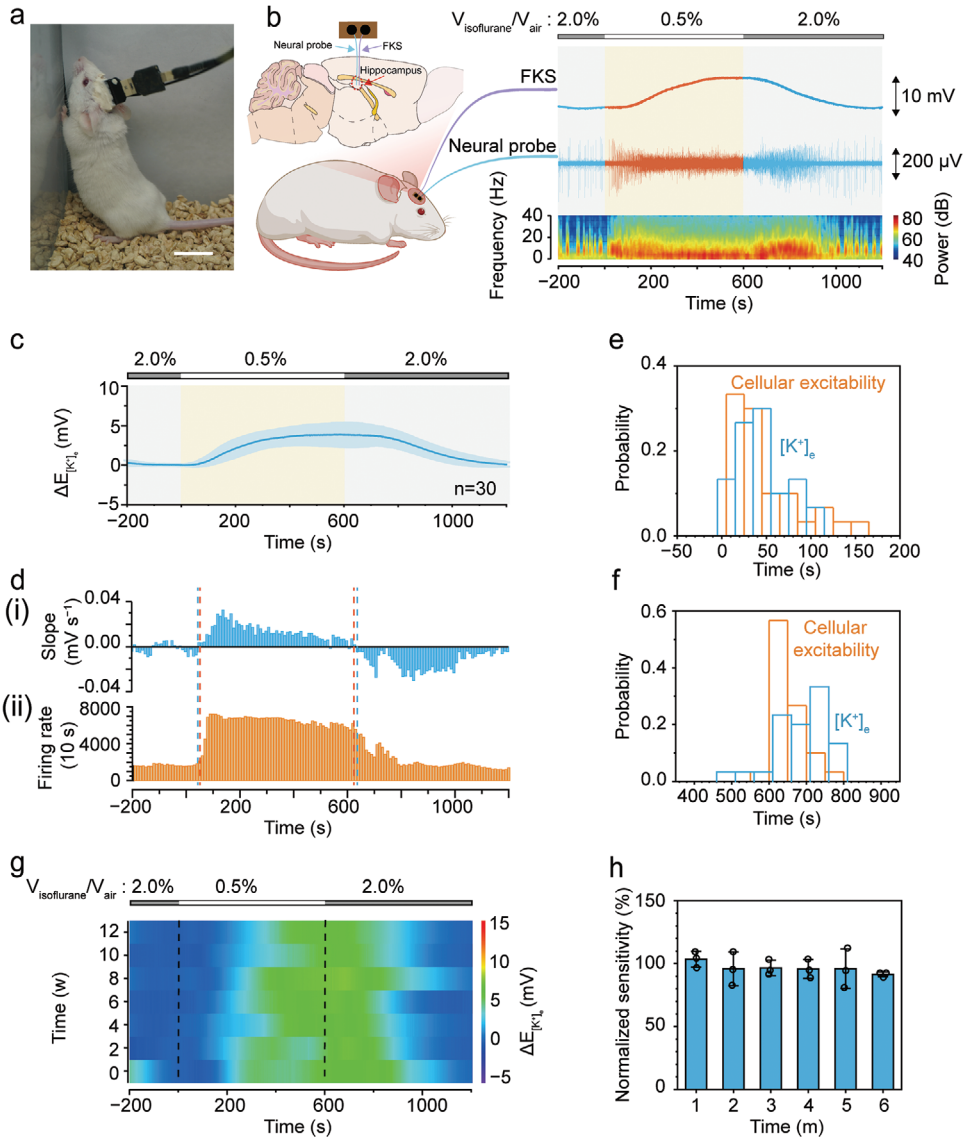

Figure 3. Simultaneous recording of $[K^+]_e$ fluctuations and electrophysiological signals using the FKS and a neural probe. a) Photograph of a freely moving mouse implanted with the FKS and a neural probe. Scale bar, 2 cm. b) FKS and neural probe being implanted into the hippocampus of the mouse brain to record extracellular K^+ ($[K^+]_e$) dynamics and electrophysiological signals (0–125 Hz), respectively. The anesthetic concentration was switched between 2% and 0.5% ($V_{isoflurane}$: V_{air}). The power density spectrum (bottom) was derived from the recorded electrophysiological signal. c) Potential changes in the FKS in response to $[K^+]_e$ fluctuations ($\Delta E_{[K^+]_e} = E_{[K^+]_e} - E_{[K^+]_{e0}}$, $n = 30$). The blue curve represents the averaged $\Delta E_{[K^+]_e}$, and the light blue shading indicates the s.d. d) The slope of $\Delta E_{[K^+]_e}$ and the firing rate of the electrophysiological signal were calculated to identify the switching times of $[K^+]_e$ and cellular excitability. i) Slope ($\Delta E/\Delta t$, $\Delta t = 10$ s, mV s^{-1}) of $\Delta E_{[K^+]_e}$, and ii) firing rates counted from the electrophysiological signal. Blue dashed and orange dashed lines represent the switching times of $[K^+]_e$ and cellular excitability, respectively. The switching time of $[K^+]_e$ is close to that of cellular excitability. e) Histogram depicting the time distributions for the $[K^+]_e$ increase (blue) and cell excitation (orange). f) Histogram depicting the time distributions for the $[K^+]_e$ decrease (blue) and cell inhibition (orange). g) Color map of $\Delta E_{[K^+]_e}$ under anesthetic regulation recorded for one mouse across 12 weeks. The results illustrate the working stability of the FKS in the brain. h) Postcalibration sensitivities ($n = 3$, mean ± s.d.) of the FKS after being implanted in the brain for 1 to 6 months. The sensitivities maintained at ≈92%. The K^+ concentrations of the test solutions were in the range of 0.5–15.5 mM.

correlation between $[K^+]_e$ fluctuations and cellular excitability transitions. A statistical histogram depicted that $[K^+]_e$ mainly increased at 0–60 s and the cells were excited at 10–60 s (Figure 3e). Likewise, a decrease in $[K^+]_e$ was observed at 610–760 s with cellular inhibition at 600–700 s (Figure 3f). These results emphasize a direct correlation between fluctuations in $[K^+]_e$ and shifts in cellular excitability, with the timing of $[K^+]_e$ alterations closely aligning with that of cellular excitability changes.

In addition, the accuracy of FKS was confirmed by the consistent data from ex situ measurements of interstitial fluid samples by clinical method (Figure S8, Supporting Information). Moreover, the long-term stability of the FKS in vivo was assessed by

© 2023 Wiley-VCH GmbH

15214095, 2024, 13, Downloaded from https://onlinelibrary.wiley.com/doi/10.1002/adma.202309862 by Fudan University, Wiley Online Library on [06/12/2024]. See the Terms and Conditions (https://onlinelibrary.wiley.com/terms-and-conditions) on Wiley Online Library for rules of use; OA articles are governed by the applicable Creative Commons License

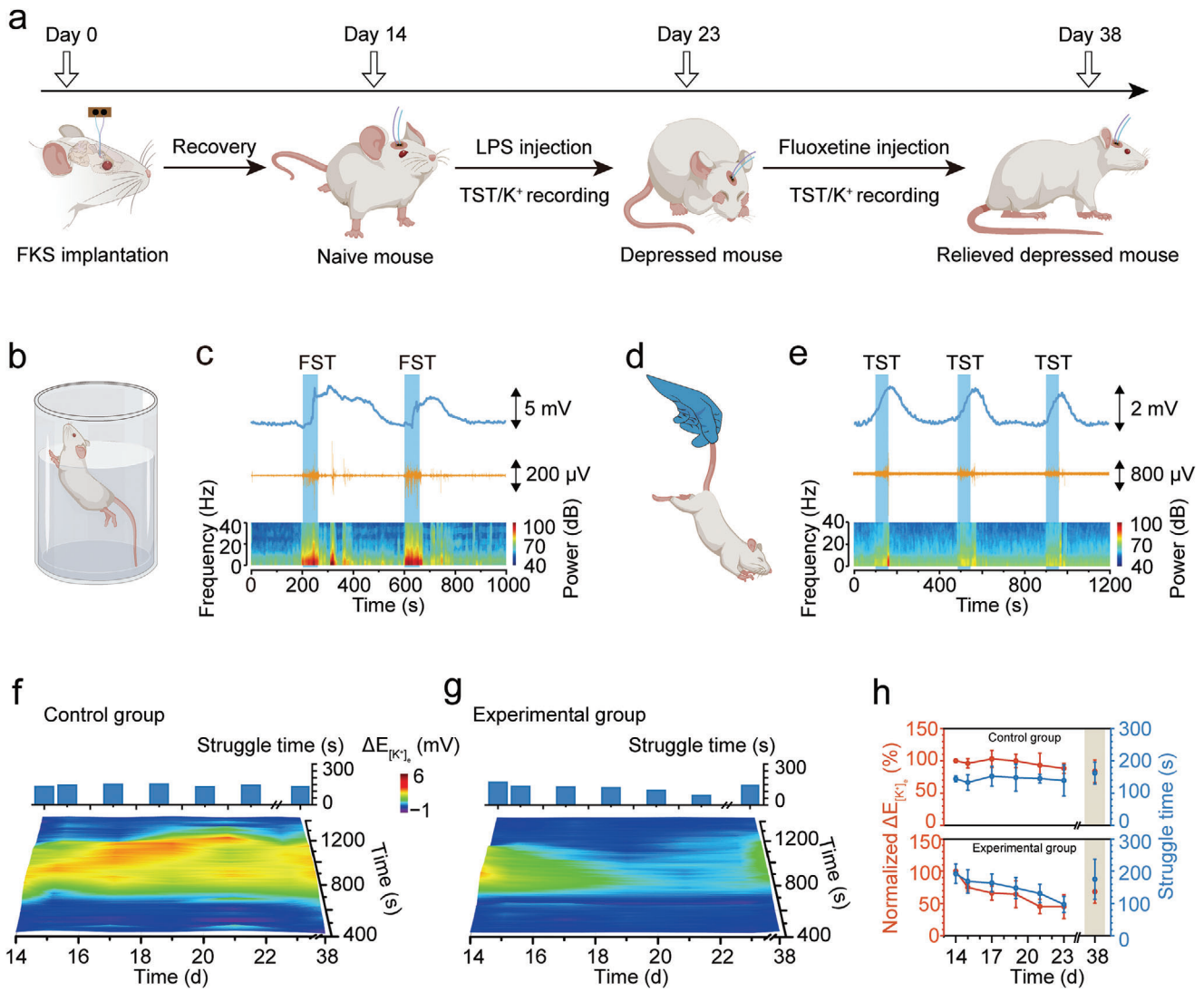

Figure 4. FKS tracked $[K^+]_e$ fluctuations along with depression-related behaviors in mice during the progression of depression. a) Schedule for the lipopolysaccharide (LPS) induced depression model and fluoxetine treatment process. After implantation of the FKS into the lateral habenula of the brain, mice recovered for 14 days and then were injected with LPS daily from days 15 to 23 and treated with fluoxetine daily from days 24 to 38. b–e) Schematic illustration and recordings of FST (b,c) and TST (d,e). The recordings include $\Delta E_{[K^+]_e}$ to show the changes in $[K^+]_e$, electrophysiological signals (0–125 Hz), and corresponding power density spectra to show cellular excitability. The results demonstrate that $[K^+]_e$ was elevated and that cells were excited in behavioral tests. f,g) Struggle time in the last 4 min in the TST and the corresponding color map of the $\Delta E_{[K^+]_e}$ recorded by the FKS in the control (f) and experimental (g) groups. Top panel, struggle time; bottom panel, color map of $\Delta E_{[K^+]_e}$. h) Normalized $\Delta E_{[K^+]_e}$ of the FKS and struggle time in the control ($n = 3$, mean ± s.d.) and experimental ($n = 3$, mean ± s.d.) groups in the TST during the whole process. $\Delta E_{[K^+]_e}$ slightly declined in the control group and, strongly decreased during depression development and increased after the treatment in the experimental group.

applying the same anesthetic modulation to induce $[K^+]_e$ fluctuations in the brain at different time points. The potential responses of the FKS presented similar trends and variations across 12 weeks, confirming its sustained working stability (Figure 3g). Meanwhile, there was no protein adsorption on the surface of the FKS after implantation for 3 and 6 months (Figure S7i,j, Supporting Information), avoiding biofouling interference with the performance of the FKS. Ultimately, after 6 months of implantation, the sensitivities of the FKS were still maintained at ≈92%, which directly confirmed the long-term stability of the FKS in the brain (Figure 3h).

Depression, as a chronic psychiatric disorder characterized by depressed mood and diminished motivation, stands as a leading cause of disability worldwide.[13] In view of this, various animal models of depression have been established to understand, diagnose, and treat this condition. For such animal models, behavioral assessments, including the tail suspension test (TST), forced swimming test (FST), and sucrose preference test (SPT), are used to estimate the extent of depression.[7d] Although the dysfunction of K^+ channels has been considered to be related to depression,[3a,e] effective monitoring of the fluctuations in $[K^+]_e$ during depression has never been achieved. Thus, the FKS and

© 2023 Wiley-VCH GmbH

15214095, 2024, 13, Downloaded from https://onlinelibrary.wiley.com/doi/10.1002/adma.202309862 by Fudan University, Wiley Online Library on [06/12/2024]. See the Terms and Conditions (https://onlinelibrary.wiley.com/terms-and-conditions) on Wiley Online Library for rules of use; OA articles are governed by the applicable Creative Commons License

a neural probe were implanted into the lateral habenula of a mouse brain to track the changes in $[K^+]_e$ during behavioral tests (**Figure** 4a). During the FST, the mouse struggled violently, and the increased amplitudes and power densities of electrophysiological signals revealed heightened cellular activity. Consistently, the sharply increased potential of the FKS indicated that $[K^+]_e$ rapidly increased (Figure 4b,c). Similar results were found during the TST (Figure 4d,e). These results indicated that $[K^+]_e$ was elevated along with increased cellular excitability during behavioral tests of mice.

Furthermore, we employed the FKS to track fluctuations in $[K^+]_e$ during the TST over the entire course of depression. For the mice in the control group, the FKS monitored $[K^+]_e$ increases of similar magnitudes due to the steady struggle times throughout the process (Figure 4f,h). In contrast, the $[K^+]_e$ fluctuations recorded from the mice in the experimental group showed notable deviations, which aligned with the depression degree. As depression progressed from days 15 to 23, the struggle time in TST gradually decreased, and the fluctuations in $[K^+]_e$ accordingly declined. When depression was relieved on day 38, the struggle time in TST increased, accompanied by an elevation of $[K^+]_e$ fluctuations (Figure 4g,h). The long-term recordings from the FKS represented a consistent alignment between the $[K^+]_e$ fluctuations and the struggle time of depression-diseased mice throughout the experiment, demonstrating the potential of using $[K^+]_e$ fluctuation as a biochemical indicator for depression.

Since $[K^+]_e$ could be modulated by the anesthetic concentration and fluctuates with the degree of depression, we proposed monitoring $[K^+]_e$ fluctuations under different anesthetic concentrations to assess the depression degree from a new biochemical perspective. The mice were implanted with the FKS and recovered for 14 days (Stage I), followed by unpredictable chronic mild stress treatment for 28 days (Stage II) (Figure S9a, Supporting Information). In the control group, under anesthetic modulation, the fluctuations in $[K^+]_e$ in Stage II were maintained at ≈98% of the value in Stage I (Figure S9b,d, Supporting Information). In the experimental group, the $[K^+]_e$ fluctuations in Stage II apparently declined to 62% of those in Stage I (Figure S9c,d, Supporting Information). The depression degree was estimated by behavioral tests, including TST, FST, and SPT (Figure S9e–g, Supporting Information), which showed consistent results with the fluctuations in $[K^+]_e$. Hence, the FKS could monitor the fluctuations in $[K^+]_e$ during the depression process and serve as an effective measurement for in-depth study of depression.

3. Conclusion

In this article, we demonstrated a fiber K^+ sensor with a long-term stability of 6 months in vivo, superior to previously reported K^+ sensors and matching the periods of chronic neuropsychiatric diseases. Utilizing this FKS, we studied the fluctuations in $[K^+]_e$ under various physiological states of mice. Furthermore, the long-term stability of the FKS enabled its ground-breaking application in depression-diseased mice to illustrate the consistency between $[K^+]_e$ fluctuations and behavioral signatures, exhibiting its potential as a powerful tool for investigating depression from the view of biochemicals. The FKS is promising to combine with other monitoring tools in vivo, for example, optical fibers, to broaden its application in revealing the pathogenic mechanisms and estimating the therapeutic effect of new medicine for neuropsychiatric diseases.

Supporting Information

Supporting Information is available from the Wiley Online Library or from the author.

Acknowledgements

This work was supported by MOST (2022YFA1203001, 2022YFA1203002), NSFC (52122310, 22075050, T2321003, 22335003, T2222005, 22175042), and STCSM (21511104900, 20JC1414902). The authors thank the Shanghai Supercomputer Center for the support of the finite element analysis.

Conflict of Interest

The authors declare no conflict of interest.

Data Availability Statement

The data that support the findings of this study are available from the corresponding author upon reasonable request.

Keywords

chronic neuropsychiatric diseases, depression, fiber electronics, implantable sensor, potassium ion

Received: September 22, 2023
Revised: November 22, 2023
Published online: December 22, 2023

[1] R. Rasmussen, J. O'donnell, F. Ding, M. Nedergaard, *Prog. Neurobiol.* **2020**, *193*, 101802.
[2] a) F. Ding, J. O'donnell, Q. Xu, N. Kang, N. Goldman, M. Nedergaard, *Science* **2016**, *352*, 550; b) P. Kofuji, E. A. Newman, *Neuroscience* **2004**, *129*, 1043; c) L. Luan, J. T. Robinson, B. Aazhang, T. Chi, K. Yang, X. Li, H. Rathore, A. Singer, S. Yellapantula, Y. Fan, Z. Yu, C. Xie, *Neuron* **2020**, *108*, 302; d) P.-Y. Shih, L. P. Savtchenko, N. Kamasawa, Y. Dembitskaya, T. J. Mchugh, D. A. Rusakov, R. Shigemoto, A. Semyanov, *Cell Rep.* **2013**, *5*, 941; e) R. Rasmussen, E. Nicholas, N. C. Petersen, A. G. Dietz, Q. Xu, Q. Sun, M. Nedergaard, *Cell Rep.* **2019**, *28*, 1182.
[3] a) Y. Cui, Y. Yang, Z. Ni, Y. Dong, G. Cai, A. Foncelle, S. Ma, K. Sang, S. Tang, Y. Li, Y. Shen, H. Berry, S. Wu, H. Hu, *Nature* **2018**, *554*, 323; b) A. H. V. Schapira, K. R. Chaudhuri, P. Jenner, *Nat. Rev. Neurosci.* **2017**, *18*, 435; c) X. Tong, Y. Ao, G. C. Faas, S. E. Nwaobi, J.i Xu, M. D. Haustein, M. A. Anderson, I. Mody, M. L. Olsen, M. V. Sofroniew, B. S. Khakh, *Nat. Neurosci.* **2014**, *17*, 694; d) T. J. Jentsch, C. A. Hübner, J. C. Fuhrmann, *Nat. Cell Biol.* **2004**, *6*, 1039; e) P. Kumar, D. Kumar, S. K. Jha, N. K. Jha, R. K. Ambasta, *Adv. Protein Chem. Struct. Biol.* **2016**, *103*, 97.
[4] a) G. Petit-Pierre, P. Colin, E. Laurer, J. Déglon, A. Bertsch, A. Thomas, B. L. Schneider, P. Renaud, *Nat. Commun.* **2017**, *8*, 1239; b) M. L. Rogers, C. L. Leong, S. A.n Gowers, I. C. Samper, S. L. Jewell, A. Khan, L. Mccarthy, C. Pahl, C. M. Tolias, D. C. Walsh, A. J. Strong, M. G. Boutelle, *J. Cereb. Blood Flow Metab.* **2017**, *37*, 1883.

© 2023 Wiley-VCH GmbH

15214095, 2024, 13, Downloaded from https://onlinelibrary.wiley.com/doi/10.1002/adma.202309862 by Fudan University, Wiley Online Library on [06/12/2024]. See the Terms and Conditions (https://onlinelibrary.wiley.com/terms-and-conditions) on Wiley Online Library for rules of use; OA articles are governed by the applicable Creative Commons License

[5] a) M. Wei, P. Lin, Y. Chen, J.i Y. Lee, L. Zhang, F. Li, D. Ling, *Nanomedicine* **2020**, *15*, 2871; b) J. Liu, F. Li, Y.i Wang, L. Pan, P. Lin, B.o Zhang, Y. Zheng, Y. Xu, H. Liao, G. Ko, F. Fei, C. Xu, Y. Du, K. Shin, D. Kim, S.-S. Jang, H. J. Chung, H.e Tian, Q.i Wang, W. Guo, J.-M. Nam, Z. Chen, T. Hyeon, D. Ling, *Nat. Nanotechnol.* **2020**, *15*, 321; c) J. Liu, L. Pan, C. Shang, B. Lu, R. Wu, Y. Feng, W. Chen, R. Zhang, J. Bu, Z. Xiong, W. Bu, J. Du, J. Shi, *Sci. Adv.* **2020**, *6*, eaax9757.

[6] a) J. Hu, A. Stein, P. Bühlmann, *TrAC, Trends Anal. Chem.* **2016**, *76*, 102; b) J. Moon, Y. Ha, M. Kim, J. Sim, Y. Lee, M. Suh, *Anal. Chem.* **2016**, *88*, 8942; c) F. Zhao, Y. Liu, H. Dong, S. Feng, G. Shi, L. Lin, Y. Tian, *Angew. Chem., Int. Ed.* **2020**, *59*, 10426.

[7] a) H. Qian, X. Kang, J. Hu, D. Zhang, Z. Liang, F. Meng, X. Zhang, Y. Xue, R. Maimon, S. F. Dowdy, N. K. Devaraj, Z. Zhou, W. C. Mobley, D. W. Cleveland, X.-D. Fu, *Nature* **2020**, *582*, 550; b) M. P. Parsons, M. P. Vanni, C. L. Woodard, R. Kang, T. H. Murphy, L. A. Raymond, *Nat. Commun.* **2016**, *7*, 11251; c) V. Alexandrov, D. Brunner, L. B. Menalled, A. Kudwa, J. Watson-Johnson, M. Mazzella, I. Russell, M. C. Ruiz, J. Torello, E. Sabath, A. Sanchez, M. Gomez, I. Filipov, K. Cox, M. Kwan, A. Ghavami, S. Ramboz, B. Lager, V. C. Wheeler, J. Aaronson, J. Rosinski, J. F. Gusella, M. E. Macdonald, D. Howland, S. Kwak, *Nat. Biotechnol.* **2016**, *34*, 838; d) S. Liu, J. Xiu, C. Zhu, K. Meng, C. Li, R. Han, T. Du, L. Li, L. Xu, R. Liu, W. Zhu, Y. Shen, Q.i Xu, *Nat. Commun.* **2021**, *12*, 6937; e) J.u-H. Lee, D.-S. Yang, C. N. Goulbourne, E. Im, P. Stavrides, A. Pensalfini, H. Chan, C. Bouchet-Marquis, C. Bleiwas, M. J. Berg, C. Huo, J. Peddy, M. Pawlik, E. Levy, M. Rao, M. Staufenbiel, R. A. Nixon, *Nat. Neurosci.* **2022**, *25*, 688; f) J. Ying, A. T. Keinath, R. Lavoie, E. Vigneault, S. El Mestikawy, M. P. Brandon, *Nat. Commun.* **2022**, *13*, 886; g) Q. Sun, J. Zhang, A. Li, M. Yao, G. Liu, S. Chen, Y. Luo, Z. Wang, H. Gong, X. Li, Q. Luo, *Nat. Commun.* **2022**, *13*, 998.

[8] a) Y. Shao, Y. Ying, J. Ping, *Chem. Soc. Rev.* **2020**, *49*, 4405; b) J. Bobacka, A. Ivaska, A. Lewenstam, *Chem. Rev.* **2008**, *108*, 329.

[9] X. Zhang, F. Shi, J. Niu, Y. Jiang, Z. Wang, *J. Mater. Chem.* **2008**, *18*, 621.

[10] a) M. Fibbioli, W. E. Morf, M. Badertscher, N. F. De Rooij, E. Pretsch, *Electroanalysis* **2000**, *12*, 1286; b) L. Zhao, Y. Jiang, H. Wei, Y. Jiang, W. Ma, W. Zheng, A.n-M. Cao, L. Mao, *Anal. Chem.* **2019**, *91*, 4421.

[11] a) I. Dietzel, U. Heinemann, G. Hofmeier, H. D. Lux, *Exp. Brain Res.* **1980**, *40*, 432; b) E. Syková, S. Rothenberg, I. Krekule, *Brain Res.* **1974**, *79*, 333.

[12] a) S. P. Lacour, G. Courtine, J. Guck, *Nat. Rev. Mater.* **2016**, *1*, 16063; b) R. Feiner, T. Dvir, *Nat. Rev. Mater.* **2018**, *3*, 17076; c) J. W. Salatino, K. A. Ludwig, T. D. Y. Kozai, E. K. Purcell, *Nat. Biomed. Eng.* **2017**, *1*, 862.

[13] A. Gururajan, A. Reif, J. F. Cryan, D. A. Slattery, *Nat. Rev. Neurosci.* **2019**, *20*, 686.

© 2023 Wiley-VCH GmbH

15214095, 2024, 13, Downloaded from https://onlinelibrary.wiley.com/doi/10.1002/adma.202309862 by Fudan University, Wiley Online Library on [06/12/2024]. See the Terms and Conditions (https://onlinelibrary.wiley.com/terms-and-conditions) on Wiley Online Library for rules of use; OA articles are governed by the applicable Creative Commons License